


# Dynamic Nuclear Polarization Enhanced NMR Spectroscopy for Pharmaceutical Formulations

## Journal Article

### Author(s):

Rossini, Aaron J.; Widdifield, Cory M.; Zagdoun, Alexandre; Lelli, Moreno; Schwarzwälder, Martin; Copéret, Christophe ; Lesage, Anne; Emsley, Lyndon

### Publication date:

2014-02-12

### Permanent link:

<https://doi.org/10.3929/ethz-b-000080771>

### Rights / license:

In Copyright - Non-Commercial Use Permitted

### Originally published in:

Journal of the American Chemical Society 136(6), <https://doi.org/10.1021/ja4092038>



# Dynamic Nuclear Polarization Enhanced NMR Spectroscopy for Pharmaceutical Formulations

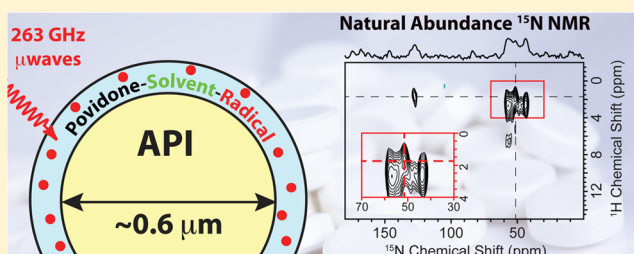
Aaron J. Rossini,<sup>†</sup> Cory M. Widdifield,<sup>†</sup> Alexandre Zagdoun,<sup>†</sup> Moreno Lelli,<sup>†</sup> Martin Schwarzwälder,<sup>‡</sup> Christophe Copéret,<sup>‡</sup> Anne Lesage,<sup>†</sup> and Lyndon Emsley<sup>\*,†</sup>

<sup>†</sup>Centre de RMN à Très Hauts Champs, Institut de Sciences Analytiques, Université de Lyon (CNRS/ENS Lyon/UCB Lyon 1), 69100 Villeurbanne, France

<sup>‡</sup>Department of Chemistry, Laboratory of Inorganic Chemistry, ETH Zürich, CH-8093 Zürich, Switzerland

## S Supporting Information

**ABSTRACT:** Dynamic nuclear polarization (DNP) enhanced solid-state NMR spectroscopy at 9.4 T is demonstrated for the detailed atomic-level characterization of commercial pharmaceutical formulations. To enable DNP experiments without major modifications of the formulations, the gently ground tablets are impregnated with solutions of biradical polarizing agents. The organic liquid used for impregnation (here 1,1,2,2-tetrachloroethane) is chosen so that the active pharmaceutical ingredient (API) is minimally perturbed. DNP enhancements ( $\epsilon$ ) of between 40 and 90 at 105 K were obtained for the microparticulate API within four different commercial formulations of the over-the-counter antihistamine drug cetirizine dihydrochloride. The different formulations contain between 4.8 and 8.7 wt % API. DNP enables the rapid acquisition with natural isotopic abundances of one- and two-dimensional  $^{13}\text{C}$  and  $^{15}\text{N}$  solid-state NMR spectra of the formulations while preserving the microstructure of the API particles. Here this allowed immediate identification of the amorphous form of the API in the tablet. API–excipient interactions were observed in high-sensitivity  $^1\text{H}$ – $^{15}\text{N}$  correlation spectra, revealing direct contacts between povidone and the API. The API domain sizes within the formulations were determined by measuring the variation of  $\epsilon$  as a function of the polarization time and numerically modeling nuclear spin diffusion. Here we measure an API particle radius of  $0.3\ \mu\text{m}$  with a single particle model, while modeling with a Weibull distribution of particle sizes suggests most particles possess radii of around  $0.07\ \mu\text{m}$ .



## 1. INTRODUCTION

The characterization of the composition and structure of formulated multicomponent materials in general, and of pharmaceutical formulations in particular, is of great industrial importance today, yet in many respects it remains an unsolved analytical challenge. While several methods can be used as indirect probes of the properties of formulations, there are very few direct probes available. On the other hand, today solid-state NMR (together with diffraction methods) is frequently used to probe the solid-state structures of pure active pharmaceutical ingredients (APIs), often in the context of identifying structural polymorphs.<sup>1–5</sup> In this respect, solid-state NMR spectroscopy would appear to be a potentially powerful direct probe of structure for formulations.

In favorable cases, three-dimensional crystal structures can be determined from pure powdered samples by solid-state NMR with the NMR crystallography approach. This is accomplished either by directly measuring internuclear distances/proximities (e.g.,  $^1\text{H}$ – $^1\text{H}$ ,  $^1\text{H}$ – $^{13}\text{C}$ ,  $^{29}\text{Si}$ – $^{29}\text{Si}$ , etc.)<sup>6–10</sup> or by comparing trial structures and computed NMR parameters and/or distances with observed parameters and/or internuclear distance constraints.<sup>11–22</sup> A number of other solid-state NMR techniques exploiting quadrupolar or uncommon spin-1/2

nuclei such as  $^7\text{Li}$ ,  $^{14}\text{N}$ ,  $^{15}\text{N}$ ,  $^{17}\text{O}$ ,  $^{19}\text{F}$ ,  $^{23}\text{Na}$ ,  $^{35}\text{Cl}$ , etc., have also been demonstrated as probes of structure and dynamics for organic solids.<sup>23–36</sup>

While all of these NMR based techniques have been successfully demonstrated for the characterization of pure crystalline powdered solids, it would be of great interest to extend these techniques to the characterization of APIs in formulations. This could enable solid-state NMR structure determination “*in situ*”, allowing polymorph screening and identification, quantification of the degree of crystallinity of the API, measurement of domain sizes, and/or the determination of API–excipient interactions. Characterization of these properties is especially important, since they influence the activity/release properties of the formulations, and the overall stability of the API phase.<sup>30,37–40</sup> However, the characterization of formulated APIs by solid-state NMR is often challenging due to the combination of the intrinsically low sensitivity of NMR, long longitudinal relaxation times,<sup>41,42</sup> and the low API content of many formulations (typically between 5 and 10 wt %).

**Received:** September 5, 2013

**Published:** January 10, 2014



Table 1. Sample Characteristics, Measured DNP Enhancements, and Relaxation Properties

sample name and composition of the impregnating liquid	brand name/ retailer	tablet mass (mg)	initial API content <sup>a</sup> (wt %)	$\epsilon_{\text{C CP}}^b$	$T_{\text{DNP}}(^1\text{H})^c$ (s)	$^{13}\text{C}$ sensitivity <sup>d</sup> ( $\text{s}^{-1/2}$ )
crystalline cetirizine dihydrochloride A (16 mM TEKPol, TCE- $d_2$ -20%) <sup>e</sup>	Sigma-Aldrich	—	100	31	22	74
crystalline cetirizine dihydrochloride A (298 K, no DNP, 16.45 T)	Sigma-Aldrich	—	100	—	24	0.2
polyvinylpyrrolidone (povidone, P) (24 mM TEKPol, TCE- $d_2$ -26%)	—	—	0	10	2.3	39
formulation F1 (24 mM TEKPol, TCE- $d_2$ -26%)	Life	115.1	8.7	64	2.2	21.5
formulation F2 (16 mM TEKPol, TCE- $d_2$ -20%)	CVS	207.2	4.8	90	2.9	7.8
formulation F3 (16 mM TEKPol, TCE- $d_2$ -20%)	Reactine	170.3	5.9	62	4.2	5.5
formulation F4 (16 mM TEKPol, TCE- $d_2$ -20%)	Wal-Zyr	181.2	5.5	40	6.5	3.1
formulation F1 (115 K, no radical solution, 11.7 T)	Life	115.1	8.7	—	6.6	0.6

<sup>a</sup>The listed API dose of 10 mg was used for the calculation. <sup>b</sup> $\epsilon_{\text{C CP}}$  is the DNP enhancement measured with  $^1\text{H}$ – $^{13}\text{C}$  cross-polarization. It usually matches the proton DNP enhancement ( $\epsilon_{\text{H}}$ ), since all of the polarization is derived from protons. <sup>c</sup> $T_{\text{DNP}}$  is the signal build-up rate constant measured with  $^1\text{H}$  saturation recovery experiments with  $^{13}\text{C}$  CPMAS for signal detection and microwave irradiation to drive DNP. The polarization time was varied from 0.5 to 20 s.  $T_1$  is reported for the 298 K experiment rather than  $T_{\text{DNP}}$ . <sup>d</sup>Sensitivity =  $[\text{SNR} \times (\tau_{\text{opt}} \times \text{NS})^{-1/2}]$ , where SNR is the measured signal-to-noise ratio of the API resonance (or most intense resonance for povidone and pure API) acquired with a polarization delay near to that providing optimal sensitivity ( $\tau_{\text{opt}} = 1.3 \times T_{\text{DNP}}$ ) and NS is the number of scans/transients. 80 Hz of exponential line broadening was applied to the spectra of the formulations prior to Fourier transformation. For the spectra of crystalline cetirizine dihydrochloride acquired with DNP at 105 K (at 9.4 T) and acquired at 298 K (at 16.4 T), 20 and 30 Hz of exponential line broadening were applied, respectively. <sup>e</sup>The percentage of  $^2\text{H}$  labeled TCE in the radical solution is indicated.

Early solid-state NMR studies of formulated pharmaceuticals were performed on aspirin (2-acetoxybenzoic acid) and paracetamol (*N*-(4-hydroxyphenyl)ethanamide), because of the importance of these drugs, the very high API contents (>30 wt %), and limited number of excipients.<sup>43–45</sup> Byrn and co-workers subsequently demonstrated that natural abundance  $^{13}\text{C}$  CPMAS NMR spectra of formulated APIs with contents as low as 5 wt % could be acquired in 8–12 h.<sup>37</sup> Subsequent experiments demonstrated that natural abundance  $^{13}\text{C}$  solid-state NMR can be applied to formulated APIs with contents as low as 0.5 wt %; however, acquisition times are usually long (~12–24 h).<sup>25,38,39,46</sup> For these reasons, subsequent solid-state NMR studies of formulated APIs have exploited highly receptive nuclei and/or proton detection,<sup>25,31,47–50</sup> have been performed on formulations with relatively high API contents<sup>43–46,51</sup> (>10 wt %), or used model formulations with a limited number of excipients.<sup>39,40,46,51</sup> Studies of formulations containing many excipients and/or low API contents are relatively rare.<sup>31,37,47,52–54</sup>

More importantly, the  $^1\text{H}$  and  $^{13}\text{C}$  solid-state NMR spectra of formulations generally possess many overlapping resonances from the large number of constituents, and multidimensional NMR spectra are generally required to restore spectral resolution and information content. Moreover, multidimensional methods are often essential to probe API–excipient interactions, or any of the other structural features discussed above. In formulations where resolution is high enough to permit  $^1\text{H}$  NMR experiments<sup>47</sup> or highly receptive nuclei are present (such as  $^{19}\text{F}$  and  $^{23}\text{Na}$ ), multidimensional experiments are possible even at low API loadings.<sup>23,25,31,36</sup> However, the low sensitivity of NMR usually precludes multidimensional acquisitions at natural isotopic abundance for  $^{13}\text{C}$  and  $^{15}\text{N}$  (to our knowledge, multidimensional  $^{13}\text{C}$  experiments have only been previously reported for model formulations with high API contents >30 wt %),<sup>27,48,49,51,53,55</sup> and thus, low sensitivity is the key barrier to the introduction of *in situ* NMR structural characterization methods for formulations.

High field dynamic nuclear polarization (DNP) low temperature (~105 K) magic angle spinning (MAS) experiments have been demonstrated to enhance the sensitivity of

high field solid-state NMR experiments by several orders of magnitude.<sup>56,57</sup> This technique has recently been applied to characterize biological systems<sup>58–65</sup> and materials.<sup>42,66–75</sup> In such experiments, a polarizing agent, usually a stable exogenous biradical,<sup>76</sup> is *homogeneously dispersed within the sample*, resulting in a uniform distribution of enhanced polarization. This is obviously not suited to the analysis of microparticulate APIs within formulations. However, it was previously shown that the protons in the bulk of nanometer sized crystallites of polypeptides could be highly polarized through proton spin diffusion when the polarizing agent is restricted only to the surface of the crystals.<sup>77</sup> We have recently generalized this concept to show how very high polarization enhancements can be obtained from ordinary crystalline organic solids impregnated with a radical containing solution, provided proton longitudinal relaxation times are long (>100 s).<sup>42</sup> This technique provides enhanced NMR sensitivity for powdered organic solids while preserving the crystal structures of the solids and the intrinsic spectral resolution. Griffin and co-workers have recently suggested that DNP experiments on amorphous organic solids (such as amorphous APIs) could be performed by including the radical during solidification/deposition of the amorphous APIs.<sup>78</sup>

Here we show that simple impregnation DNP can be applied to obtain large sensitivity enhancements for formulated pharmaceuticals. This enables the rapid acquisition of 1D and 2D  $^1\text{H}$ – $^{13}\text{C}$  and  $^1\text{H}$ – $^{15}\text{N}$  solid-state NMR spectra from drug formulations, at natural isotopic abundance, with API contents between 4.8 and 8.7 wt %. We then show that impregnation DNP can be used to determine *in situ* the distributions of domain sizes of the API in a formulation, something which was not previously possible by NMR for such a complex sample.

## 2. EXPERIMENTAL SECTION

Crystalline cetirizine dihydrochloride (A, [2-[4-[(4-chlorophenyl)-phenylmethyl]-1-piperazinyl]ethoxy]acetic acid dihydrochloride) was obtained from Sigma-Aldrich and used without further purification. Polyvinylpyrrolidone (povidone), starch,  $\alpha$ -lactose monohydrate, and hydroxypropylmethylcellulose (hypromellose) were purchased from Alfa Aesar and used without further purification. Amorphous A was

prepared by dissolving ca. 0.3 g of **A** in ca. 60 mL of 50:50 acetone:water solution within a 100 mL ceramic crucible. The volatile solvent was then allowed to evaporate overnight, producing a clear amorphous film of **A**. The four commercial formulations of the drug containing **A** as the API were purchased over the counter at different pharmacies in the USA and Canada. The commercial formulations (and manufacturers where available) were "Life Brand Extra Strength Aller-Relief" (Pharmascience, Inc.) (**F1**), "CVS Indoor/Outdoor Allergy Relief" (manufacturer not provided, product of India, distributed by CVS Pharmacy, Inc.) (**F2**), "Reactine" (Pfizer, Inc.) (**F3**), and "Walgreens WAL-ZYR All Day Allergy" (distributed by Walgreens, Co.) (**F4**). SEM images of **F1** were acquired with a LEO 1530 Gemini FEG SEM microscope.

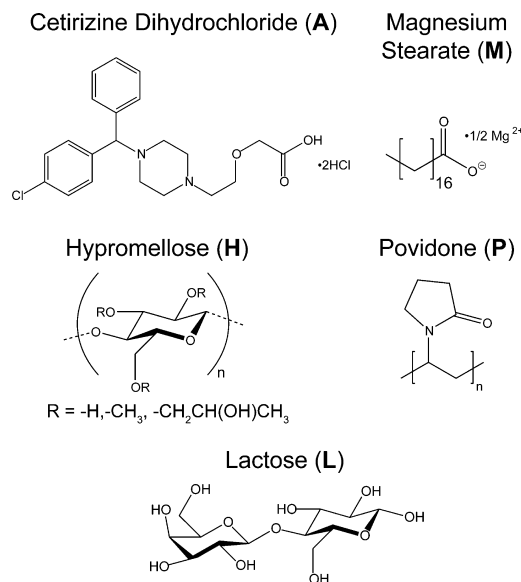
For DNP NMR experiments, typically 40–45 mg of gently ground tablet was impregnated with 20–25  $\mu\text{L}$  of a biradical solution of 1,1,2,2-tetrachloroethane (TCE). Amorphous and crystalline **A** were finely ground by hand with a mortar and pestle to reduce the particle size prior to impregnation. TEKPol<sup>79</sup> and bCTbK<sup>80</sup> nitroxide biradicals were used as polarizing agents with biradical concentrations between 14 and 24 mM. The biradical TCE solution was partially deuterated with TCE- $d_2$  in order to increase  $\epsilon$  (Table 1).<sup>80</sup>

DNP solid-state NMR experiments were performed on a widebore 400 MHz Bruker Avance III spectrometer equipped with a 263 GHz gyrotron, a low temperature cooling cabinet, and a triple resonance 3.2 mm low temperature probe.<sup>81</sup> The sample temperature for DNP experiments was approximately 105 K. The field sweep coil of the main magnetic field was set so that microwave irradiation occurred at the same position as the positive enhancement maximum for 1-(TEMPO-4-oxy)-3-(TEMPO-4-amino)propan-2-ol (TOTAPOL).<sup>76,81</sup> DNP enhancements ( $\epsilon$ ) were determined by comparing the intensity of spectra acquired with and without microwave irradiation. Additional solid-state NMR experiments were performed on 500 or 700 MHz Bruker Avance III solid-state NMR spectrometers. <sup>15</sup>N chemical shifts were referenced with respect to nitromethane by comparison to the <sup>1</sup>H resonance frequency.<sup>82</sup> CPMAS experiments were performed with a contact pulse on <sup>1</sup>H which was linearly ramped from  $\nu_1 = 66$  to 93 kHz and from 58 to 82 kHz for <sup>13</sup>C and <sup>15</sup>N experiments, respectively.<sup>83,84</sup> <sup>13</sup>C and <sup>15</sup>N CP spin lock rf field amplitudes of 57 and 42 kHz were used, respectively. The SPINAL-64 heteronuclear decoupling scheme was applied during acquisition with <sup>1</sup>H rf fields of ca. 100 kHz.<sup>85</sup> During  $t_1$  of the dipolar heteronuclear correlation (HETCOR) experiments, eDUMBO-1<sub>22</sub> homonuclear <sup>1</sup>H decoupling was applied and proton chemical shifts were corrected by applying a scaling factor of 0.57.<sup>86</sup> Low temperature experiments at 500 MHz were performed with a double resonance 3.2 mm low temperature MAS probe similar to that used for DNP. Room temperature experiments at 700 and 500 MHz employed 3.2 mm triple resonance HXY and 4 mm double resonance HX probes, respectively. Numerical spin diffusion models were constructed with MatLab v7.10 (The MathWorks, Inc.) as previously described.<sup>42</sup> Differing from the previous procedure, no reduction in the proton  $T_1$ 's at the surface of the API particles was assumed in the present case due to the small particle size and similarity of the proton  $T_1$ 's at the surface and in the core of the API particles. The MatLab code is available in the Supporting Information, or from the authors upon request.

### 3. RESULTS AND DISCUSSION

**3.1. DNP Enhanced NMR for Pharmaceutical Formulations.** **3.1.1. DNP Enhanced Solid-State NMR of Crystalline Cetirizine Dihydrochloride.** Prior to discussing results from DNP experiments on the formulated pharmaceutical, we first discuss experiments on crystalline cetirizine dihydrochloride (**A**, molecular structure depicted in Chart 1) for reference and to illustrate how DNP can improve the characterization of pure pharmaceuticals. The insolubility of crystalline **A** in solvents compatible with DNP<sup>87</sup> was screened with solution NMR spectroscopy as previously described.<sup>42</sup> **A** was found to be insoluble in both TCE and 1,4-dibromobutane.

**Chart 1. Molecular Structures of the API Cetirizine Dihydrochloride (**A**) and the Excipients Magnesium Stearate (**M**), Hydroxypropyl Methylcellulose (Hypromellose, **H**), Polyvinylpyrrolidone (Povidone, **P**), and Lactose (**L**)**



TCE was favored for the experiments here, since its lone <sup>13</sup>C NMR resonance has minimal overlap with the resonances of **A** and it usually provides higher enhancements. <sup>13</sup>C CPMAS NMR spectra of crystalline **A** with and without the addition of TEKPol TCE solution and powder X-ray diffraction patterns of crystalline **A** at 298 and 110 K suggest that neither the impregnation procedure nor the reduced sample temperature induce phase transitions in crystalline **A** (Figure S1, Supporting Information).

Figure 1 shows the DNP enhanced natural abundance <sup>13</sup>C and <sup>15</sup>N CPMAS NMR spectra of samples of crystalline **A** impregnated with 16 mM TEKPol TCE solution and cooled to  $\sim 105$  K. For crystalline **A**, a <sup>13</sup>C CPMAS DNP enhancement ( $\epsilon_{\text{CP}}$ ) of 31 was obtained with a polarization delay ( $\tau$ ) of 26 s. The proton DNP enhancement ( $\epsilon_{\text{H}}$ ) of the TCE at the surface of the crystals was about 118, as indicated by <sup>1</sup>H spin echo experiments (Figure S2, Supporting Information). The high spectral resolution and the reduced  $\epsilon$  for **A** as compared to the impregnating liquid are fully consistent with an externally impregnated crystalline organic solid.<sup>42</sup> The large gain in sensitivity enables the rapid acquisition of <sup>1</sup>H–<sup>13</sup>C and <sup>1</sup>H–<sup>15</sup>N 1D CPMAS, 2D dipolar HETCOR, and <sup>13</sup>C–<sup>13</sup>C scalar correlation (refocused INADEQUATE) solid-state NMR spectra at natural isotopic abundance (Figures 1–3 and 5 and Figure S3, Supporting Information). For example, with impregnation DNP, a one-dimensional natural abundance <sup>13</sup>C CPMAS spectrum of **A** with a high signal-to-noise ratio ( $\text{SNR} > 400$ ) was acquired in only 2 min (Figure 1A). For comparison, with standard solid-state NMR instrumentation at 298 K, a spectrum with a SNR of  $\sim 23$  required about 4.2 h (Figure S4, Supporting Information). This demonstrates the *sensitivity enhancement* of several orders of magnitude provided by impregnation DNP at 105 K for crystalline solids.<sup>42</sup>

It was also possible to rapidly acquire a one-dimensional <sup>15</sup>N CPMAS spectrum of **A** with a high SNR ( $\sim 40$ ) in only 8 min with DNP (Figure 1C). There are only two resonances in the <sup>15</sup>N CPMAS spectrum, with shifts of 59.1 and 46.4 ppm,



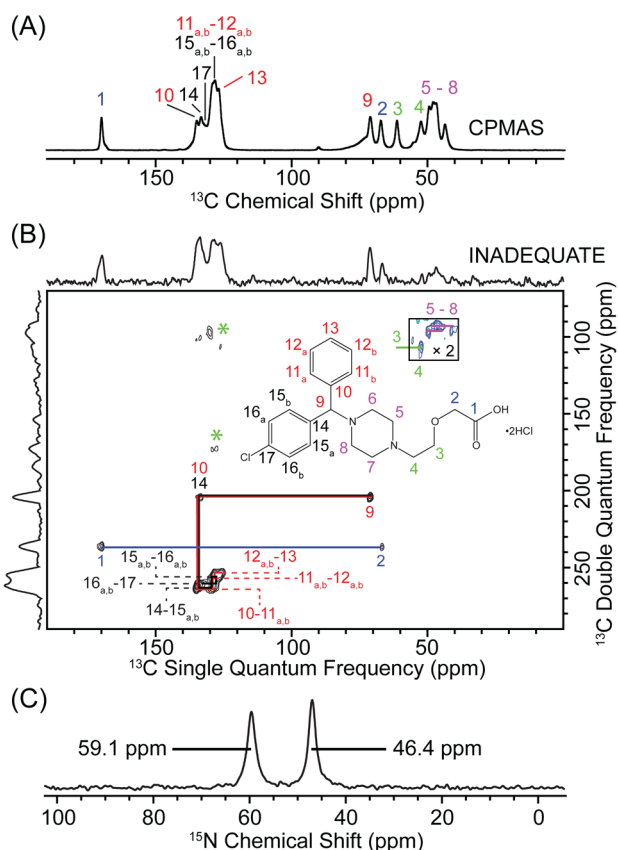


**Figure 1.** 105 K DNP enhanced natural abundance (A)  $^{13}\text{C}$  CPMAS spectrum (4 scans, 26 s  $\tau$ ), (B)  $^{13}\text{C}$ - $^{13}\text{C}$  refocused INADEQUATE correlation spectrum, and (C)  $^{15}\text{N}$  CPMAS spectrum (8 scans, 26 s  $\tau$ ) of crystalline **A** impregnated with a 16 mM solution of TEKPol in TCE (with 20%  $d_2$ -TCE). The INADEQUATE spectrum enables the assignment of the  $^{13}\text{C}$  resonances as indicated on the molecular structure drawing (assigned chemical shifts are given in Table S2, Supporting Information). The 2D spectrum was acquired in 14.2 h (32 scans per increment, a 20 s polarization delay between scans, and 80  $t_1$  increments with a 32  $\mu\text{s}$   $t_1$  increment). The States-TPPI procedure<sup>88,89</sup> was employed to achieve quadrature detection in the indirect dimension. Asterisks indicate folded-back sidebands.

corresponding to the two inequivalent nitrogen atoms in the molecule. The observation of a single set of  $^{15}\text{N}$  and  $^{13}\text{C}$  peaks suggests that there is only one molecule within the asymmetric unit cell (i.e.,  $Z' = 1$ ). To the best of our knowledge, a crystal structure for **A** has not been previously reported, nor have any polymorphs of **A** been identified.

A  $^{13}\text{C}$ - $^{13}\text{C}$  refocused INADEQUATE<sup>90</sup> correlation spectrum was acquired in only 14.2 h (Figure 1). 2D  $^1\text{H}$ - $^{15}\text{N}$  dipolar HETCOR spectra of **A** were acquired in only 27 min (Figure S4 and B). Notably, with short contact times ( $\tau_{\text{CP}}$ ), correlations are observed to acidic protons directly bound to the amine nitrogen atoms (with shifts >10 ppm in the  $^1\text{H}$  dimension) and correlations to the adjacent  $-\text{CH}_2$  protons are visible. At long contact times, additional long-range correlations to the aromatic protons are visible. The complete assignment of the  $^1\text{H}$ ,  $^{13}\text{C}$ , and  $^{15}\text{N}$  resonances for **A** resulting from this analysis is given in Table S2 (Supporting Information).

**3.1.2. DNP Enhanced NMR of Pharmaceutical Formulations.** We have applied DNP enhanced NMR to four commercially available solid formulations of the over-the-counter antihistamine drug cetirizine dihydrochloride. The

formulations contain from 4.8 to 8.7 wt % API (Table 1). All of the formulations contain the excipients polyvinylpyrrolidone (povidone, **P**), lactose (**L**), hydroxypropyl methylcellulose (hypromellose, **H**), magnesium stearate (**M**), corn starch (**S**), polyethylene glycol, and titanium dioxide (structures for some excipients are depicted in Chart 1). These are some of the most commonly encountered excipients in formulated pharmaceuticals.<sup>91</sup> In order to prepare samples for DNP, the tablets were gently ground by hand with a mortar and pestle and then impregnated with a small volume of 1,1,2,2-tetrachloroethane (TCE) solution of the nitroxide biradical TEKPol (Table S1, Supporting Information).<sup>79</sup> The impregnation DNP method is well adapted here, since just enough liquid is used so as to impregnate the sample, without creating a suspension, and thus without significantly diluting the sample.<sup>72</sup>

Ideally, the impregnation procedure should not affect the structure (phase, particle size, etc.) of the API within the formulation. However, as discussed below, here we find that the API within the tablets is present as an amorphous form rather than as a crystalline form. For these reasons, an amorphous form of **A** was also prepared and characterized by DNP and low temperature NMR experiments (*vide infra*).

While crystalline **A** is insoluble in TCE, the form of amorphous **A** prepared here was found to be soluble in TCE (by solution  $^1\text{H}$  NMR experiments, Figure S5, Supporting Information).  $^1\text{H}$  solution NMR spectra of extracts of **F1** and **F4** into a large excess of TCE indicate that up to ca. 60 and 32% of **A** can be solubilized, respectively (with less than 200 mg of ground tablet being extracted into more than 0.9 mL of TCE, Figure S6, Supporting Information). Impregnation of less than 50 mg of ground tablet with less than 30  $\mu\text{L}$  of TEKPol TCE solution for the DNP experiments should solubilize only a marginal amount of amorphous **A**. Within the formulations, a substantial fraction of the TCE solution will be absorbed by swelling of the polymeric components such as **H** and **P**. We also note that, for the DNP experiments, the ground formulations are impregnated and then quickly (less than 10 min) frozen when placed into the low temperature NMR probe for experiments. Therefore, it is unlikely that the structure of **A** within the formulation is significantly perturbed by the impregnation procedure. Consistent with this hypothesis, DNP solid-state NMR experiments on impregnated **F1** clearly indicate that amorphous **A** exists in the sample in micro-particulate domains that are externally polarized via spin diffusion (*vide infra*).

From DNP enhanced  $^{13}\text{C}$  NMR experiments on **P** and **H**, it is clear that these two polymer excipients readily swell and absorb the radical solution. It is likely that the other excipients, which are insoluble in TCE, such as **L**, **S**, and titanium dioxide, are unaffected by the impregnation. As we illustrate below, penetration of the impregnating solution into the polymer matrix surrounding the API is a highly advantageous feature of the experiments.

**3.1.3. DNP Enhanced Solid-State NMR of Pure Excipients and Formulation F1.** The DNP enhanced  $^{13}\text{C}$  CPMAS spectra of the pure excipients and of crystalline **A** and amorphous **A** are compared to the spectrum of **F1** in Figure 2. The spectra of the pure excipients enable the “background” signals from the various excipients and the signals from **A** to be assigned within the DNP enhanced  $^{13}\text{C}$  CPMAS spectrum of **F1**, as illustrated in Figure 2.

Comparison of the spectra of pure amorphous or crystalline **A** and **F1** clearly demonstrate that **A** is amorphous within **F1**

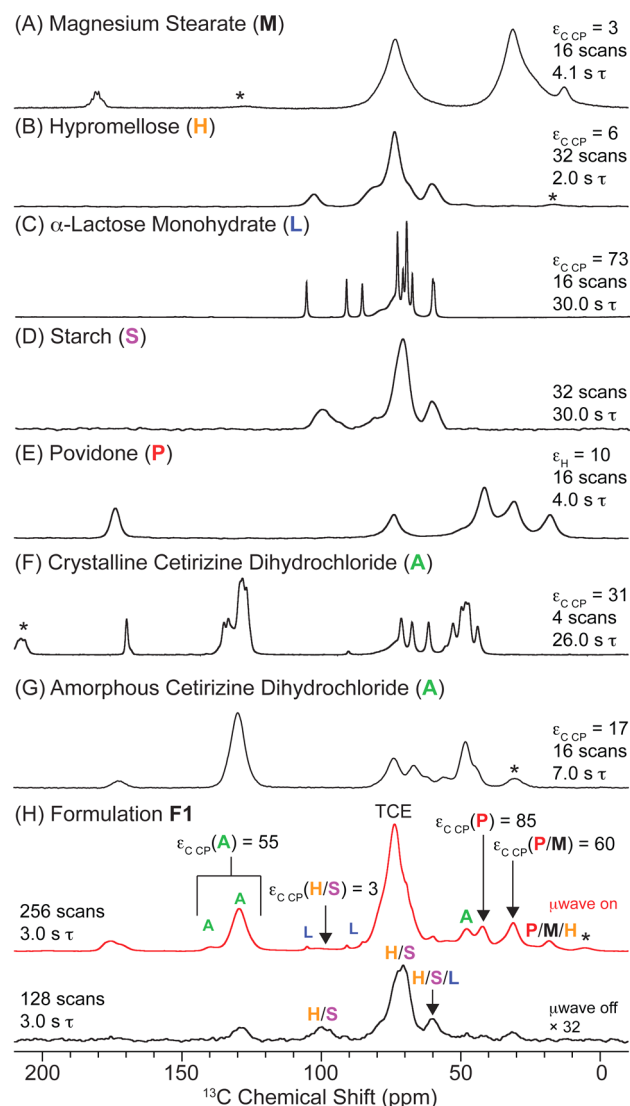


**Figure 2.** 105 K DNP enhanced natural abundance  $^{13}\text{C}$  CPMAS spectra of (A) magnesium stearate (M), (B) hypromellose (H), (C)  $\alpha$ -lactose monohydrate (L), (D) starch (S), (E) povidone (P), (F) crystalline cetirizine dihydrochloride (A), (G) amorphous cetirizine dihydrochloride (A), and (H) formulation F1. All solids were ground and impregnated with TCE solutions of TEKPol except for S where spectra were acquired from the pure solid without any DNP enhancement (Table S1, Supporting Information, provides details of sample preparation). The  $^{13}\text{C}$  CP DNP enhancement ( $\epsilon_{\text{CP}}$ ) for the compound, the number of scans, and the polarization delay ( $\tau$ ) are indicated. Asterisks denote spinning sidebands. Spectra are shown with arbitrary vertical scaling.

(and all of the other formulations, *vide infra*). Comparison of room temperature and low temperature  $^{13}\text{C}$  CPMAS experiments on F1 (and amorphous A) without the impregnating solvent (Figure S7, Supporting Information) make it clear that the broadening of the  $^{13}\text{C}$  resonances of A does not arise from the impregnation procedure (or possible partial dissolution of A, as discussed above) or from the reduction in sample temperature. Rather, A clearly exists as an amorphous phase within F1. The room temperature powder X-ray diffraction pattern of F1 does not show any reflections associated with crystalline A, also consistent with an amorphous phase of A (Figure S8, Supporting Information). Previous solid-state NMR studies of formulations indicate that crystalline API is present in

most formulations;<sup>25,31,36,39,43–46,52</sup> however, at least two studies have also observed amorphous API phases within formulated pharmaceuticals.<sup>23,54</sup> A number of solid-state NMR studies have also been performed on model amorphous API dispersions.<sup>27,40,49</sup>

The DNP enhancements  $\epsilon_{\text{CP}}$  can also be measured for the individual components of F1 with resolved/isolated  $^{13}\text{C}$  resonances, and we find significant variation between A and the different excipients. A had a relatively high  $\epsilon_{\text{CP}}$  of 55 (measured with  $\nu_{\text{rot}} = 12.5$  kHz to eliminate spinning sideband overlap), which enables  $^{13}\text{C}$  NMR signals for A to be detected with high SNR. In F1, L has an  $\epsilon_{\text{CP}}$  of 34 (with a 60 s polarization delay, Figure S9, Supporting Information), P has an  $\epsilon_{\text{CP}}$  of 85, and H/S have an  $\epsilon_{\text{CP}}$  of 3. The enhancements observed for pure H and L are similar to the enhancements observed for those excipients within F1. Pure P and M possess significantly larger  $\epsilon$  in F1 than they do in their pure forms. The difference in  $\epsilon$  for pure excipients and excipients within F1 likely reflects a change in the morphology (e.g., particulate vs molecularly dispersed) and/or concentration of the excipients. The enhancements will also likely also depend upon the concentration of the radical near the particular excipient within the formulation. The relatively low enhancements for H, S, and L in F1 are advantageous in the present case because the “background” signals from these excipients are suppressed compared to the API signal.

#### 3.1.4. DNP Enhanced Solid-State NMR of Pure Povidone.

Povidone (P) is a water-soluble polymer and is a commonly encountered pharmaceutical excipient. We focus here on P, since interactions between the API and P within formulations are hypothesized to stabilize the amorphous API and to modulate API release rates.<sup>27,49,53</sup> For P impregnated with a 24 mM solution of TEKPol in TCE, a  $\epsilon_{\text{H}}$  of  $\sim 10$  was obtained (Figure 2E). The relatively low  $\epsilon$  here probably arises from short proton longitudinal relaxation times ( $T_1 \sim 2.3$  s at 105 K), high proton concentration, and the dilution of the biradical in the swollen polymer. The low temperature DNP enhanced  $^{13}\text{C}$  CPMAS NMR spectrum is very similar to a previously reported room temperature spectrum.<sup>27,40</sup>

The DNP enhanced  $^{15}\text{N}$  CPMAS NMR spectrum possesses a single broad resonance centered at 128 ppm (Figure 3). The  $^1\text{H}$  chemical shifts observed in the  $^1\text{H}$ – $^{13}\text{C}$  and  $^1\text{H}$ – $^{15}\text{N}$  HETCOR spectra of impregnated P (Figure S10C, Supporting Information) are useful for interpreting the  $^1\text{H}$ – $^{15}\text{N}$  HETCOR spectra of F1 below. Notably, at a short CP contact time (0.25 ms), all  $^{13}\text{C}$  nuclei correlate with protons with chemical shifts between 1.0 and 1.7 ppm. With a longer CP contact time (1.5 ms), additional correlations are observed between the solvent carbon nuclei of TCE and the protons of P. These observations are consistent with swelling of the povidone by the solvent and indicate direct incorporation of TCE and TEKPol into P. The  $^1\text{H}$ – $^{15}\text{N}$  HETCOR spectrum acquired with a long CP contact time (2.5 ms) primarily shows a correlation between the single nitrogen resonance and a broad proton resonance centered at 1.8 ppm (Figure S10, Supporting Information).

**3.1.5. Sensitivity Enhancement by DNP for Pharmaceutical Formulations.** One-dimensional DNP enhanced  $^{13}\text{C}$  and  $^{15}\text{N}$  CPMAS solid-state NMR spectra of the four commercial formulations of cetirizine dihydrochloride (F1–F4, Table 1) are shown in Figure 3. All four formulations are characterized by relatively low API contents (4.8–8.7 wt % of A). The  $^{13}\text{C}$  and  $^{15}\text{N}$  CPMAS spectra of F1–F4 are broadly similar because

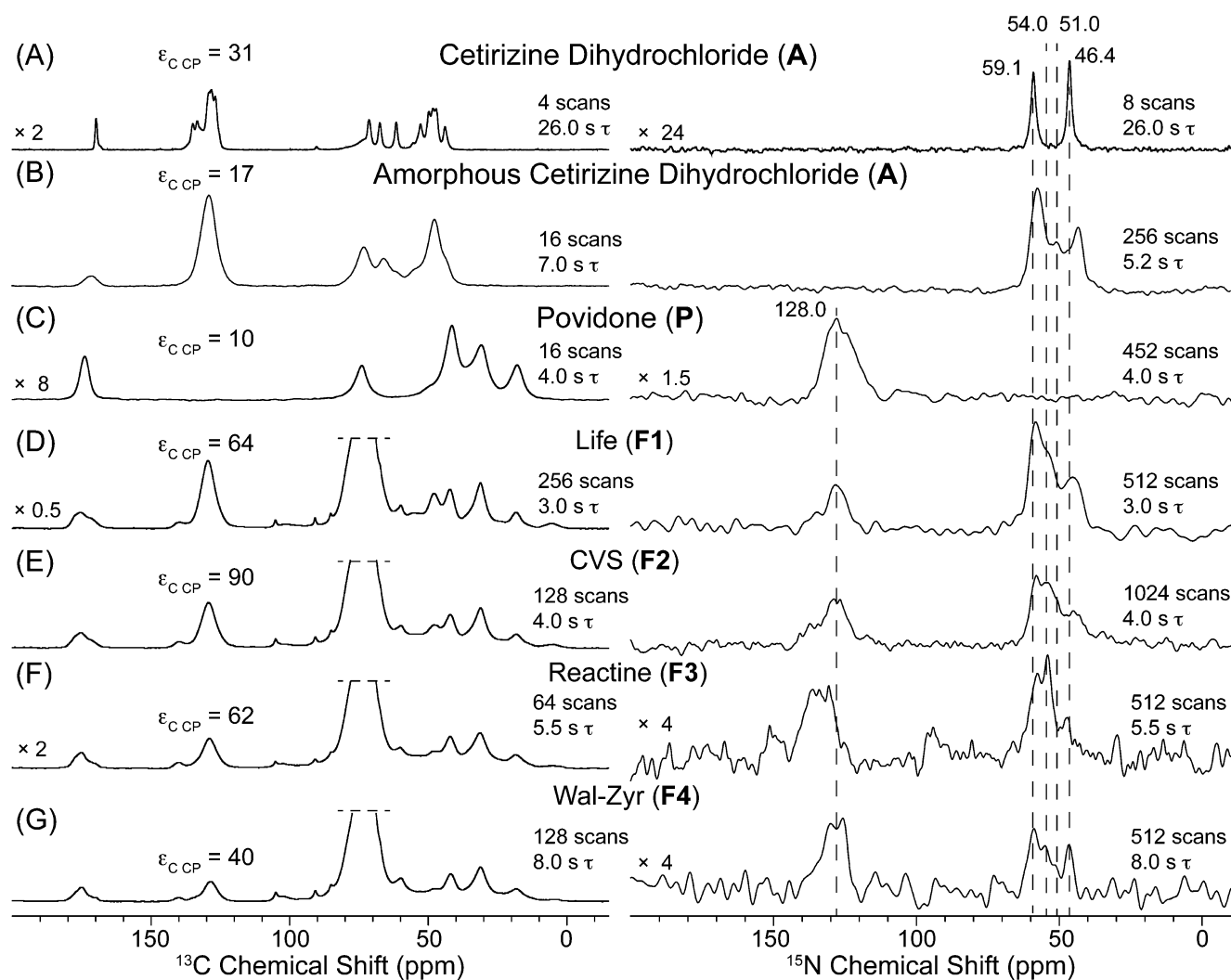


**Figure 3.** 105 K DNP enhanced natural abundance  $^{13}\text{C}$  (left column) and  $^{15}\text{N}$  (right column) CPMAS solid-state NMR spectra of (A) crystalline cetirizine dihydrochloride (A), (B) amorphous cetirizine dihydrochloride (A), (C) povidone (P), (D) “LIFE” brand formulation (F1), (E) “CVS” brand formulation (F2), (F) “Reactine” brand formulation (F3), and (G) “Wal-Zyr” brand formulation (F4) impregnated with TCE solutions of TEKPol (Table 1).  $^{13}\text{C}$  CP DNP enhancements for the API (or povidone) are listed for each spectrum, and the TCE resonance has been truncated to better illustrate low intensity signals. The number of scans and polarization delay ( $\tau$ ) used for each spectrum are indicated in the figure. All spectra were acquired with a sample spinning frequency ( $\nu_{\text{rot}}$ ) of 12500 Hz in order to eliminate sideband overlap. Note that the DNP enhancements were measured in separate experiments with  $\nu_{\text{rot}} = 8000$  Hz. Experiments on F1 indicate that  $\epsilon_{\text{C CP}}$  with a 12500 Hz spinning rate are ca. 85% of those measured at 8000 Hz.  $^{15}\text{N}$  CPMAS spectra were acquired with contact times between 2.5 and 4.0 ms.

all of the formulations contain the same ingredients (Figure 3). Notably, in all four formulations, A is amorphous, as indicated by the broad  $^{13}\text{C}$  resonances. Since none of the excipients possess aromatic carbons, the aromatic carbon resonances of A are well resolved in the  $^{13}\text{C}$  CPMAS spectra, and  $\epsilon_{\text{C CP}}$  for the API resonances can be easily measured and used for optimizing experimental conditions. The biradical concentration and TCE deuteration levels providing optimal  $\epsilon$  for the API were optimized for F1 and F3. Only a small variation of  $\epsilon$  with radical concentration and solvent deuteration level was observed (Figure S11, Supporting Information). With these conditions, large  $\epsilon_{\text{C CP}}$  values for the API of between 40 and 90 were obtained for the different formulations (measured with  $\nu_{\text{rot}} = 8$  kHz). The variation in  $\epsilon_{\text{C CP}}$  for A among F1–F4 likely arises from variations in the grain size of A, API proton longitudinal relaxation times, and the excipient concentrations at the API particle surface. High SNR 1D  $^{13}\text{C}$  CPMAS spectra could be rapidly acquired for F1–F4 because of the large  $\epsilon$  and

relatively short  $T_{\text{DNP}}$ . For example, the DNP enhanced  $^{13}\text{C}$  CPMAS spectrum of F1 was acquired in only 13 min (256 scans, 3.0 s polarization delay) with a SNR of  $\sim 600$  for the API resonance, despite the relatively low API content of 8.7 wt %. A similar sensitivity is obtained for the other formulations (Table 1). F4 possesses the lowest  $^{13}\text{C}$  NMR sensitivity due to the relatively low  $\epsilon_{\text{C CP}}$  of 40 and API content of 5.5 wt %; however, the SNR was  $\sim 145$  after 17 min (128 scans, 8.0 s polarization delay) for the API. This suggests that a 1D  $^{13}\text{C}$  CPMAS spectrum of F4 with SNR  $> 15$  could be acquired in a similar time frame even if the API wt % was reduced to levels as low as 0.5 wt %. This clearly illustrates the tremendous gain in sensitivity afforded by DNP for pharmaceutical formulations which enables the rapid acquisition of 1D and 2D  $^1\text{H}$ – $^{15}\text{N}$  CPMAS spectra of F1–F4.

**3.2. DNP Enhanced NMR to Probe the Microstructure of Formulations.** The gain in sensitivity provided by the impregnation DNP method described above allows us to



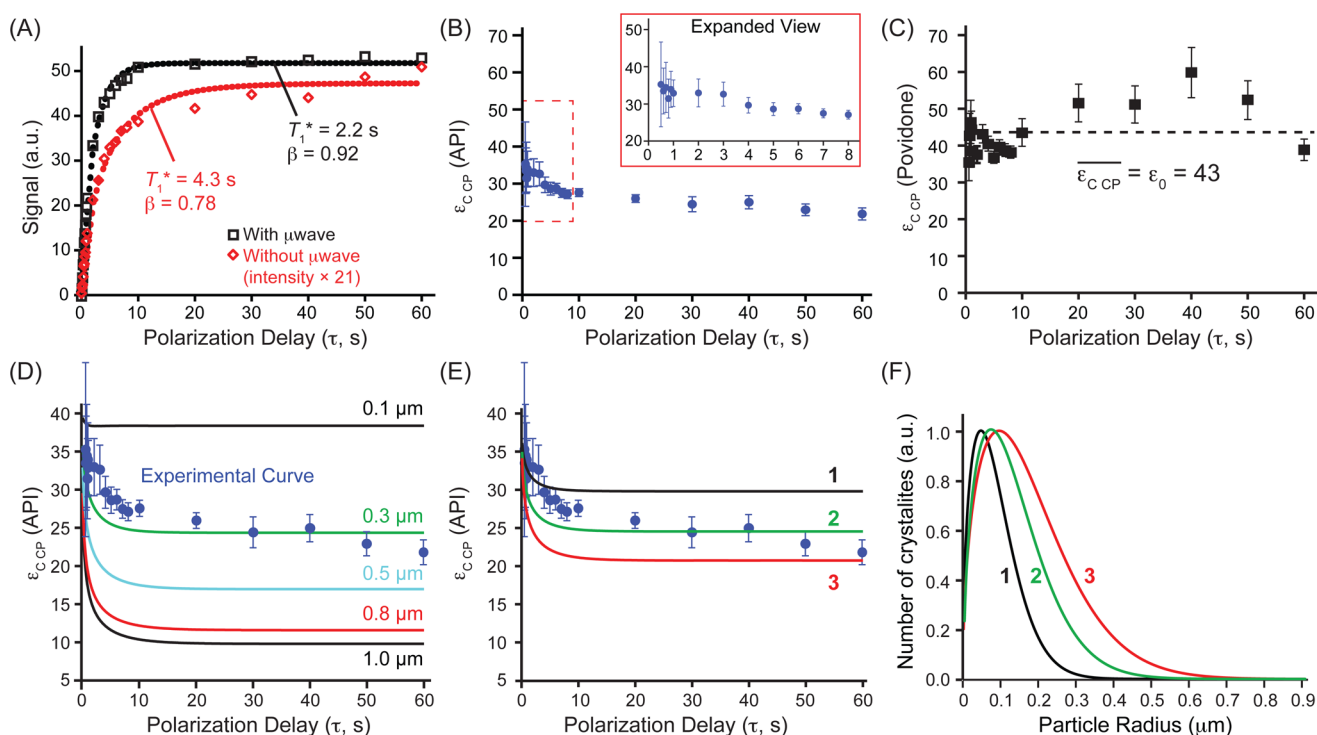


**Figure 4.** (A) Signal build-ups observed for **F1** with a saturation recovery CP pulse sequence with (black) and without (red) microwave irradiation. Curves were fit with stretched exponential functions of the form  $S(t) = S_0 \times [\exp(-(t/T_1^*)^\beta)]$ . The values of  $T_1^*$  and  $\beta$  are indicated. (B) The measured values of  $\epsilon_{CP}$  for the API resonance of **F1** at 128 ppm as a function of polarization time. The inset shows  $\epsilon_{CP}$  at short  $\tau$ . Error bars were calculated by propagation of error using the noise levels of the spectra acquired with and without microwave irradiation as the standard deviation. (C) Measured values of  $\epsilon_{CP}$  for the povidone resonance of **F1** at 41.5 ppm. The average value of  $\epsilon_{CP}$  for **P** was 43, and this was assumed to be the enhancement at the surface of the API particles ( $\epsilon_0$ ). (D) Comparison between experimental and simulated  $\epsilon$  of the API as a function of  $\tau$  using a numerical model of spin diffusion for spherical particles of the indicated radius (see ref 42 for more details). (E) Simulations of the variation of  $\epsilon$  for different Weibull distributions of the particle radius. (F) Plots of the Weibull distributions of the particle radius used in part E. Weibull distributions 1, 2 and 3 employed shape parameters ( $k$ ) of 1.5 and the center of the distributions ( $\lambda$ ) was 0.10, 0.15 and 0.20  $\mu\text{m}$ , respectively. For all simulations, the surface enhancement ( $\epsilon_0$ ) was fixed at 43, the proton longitudinal relaxation time ( $T_1$ ) of the API was 5.3 s, the  $T_1$  at the surface of the particles was set to 2.3 s to match the  $T_1$  measured for povidone, and the diffusion constant ( $D$ ) was  $1.0 \times 10^5 \text{ \AA}^2 \text{ s}^{-1}$ .

envisage NMR approaches to determine some key properties of formulations. Here we show how DNP enhanced NMR enables previously inaccessible measurements of (i) the API domain sizes and (ii) API–excipient interactions between the domains. For these in-depth analyses, we focus on **F1**, since it has the highest **A** content which reduces the required spectrometer time. However, the sensitivity is high enough with DNP that it would certainly be possible to perform such experiments for the other formulations with lower **A** content.

**3.2.1. Measuring API Domain Sizes with DNP.** In DNP experiments where the radical is homogeneously distributed and the cross effect is the dominant polarization mechanism,  $\epsilon$  is usually constant regardless of the polarization delay ( $\tau$ ). However, in our previous study on slowly relaxing externally impregnated crystalline solids, we observed that  $\epsilon$  significantly decreases to a plateau value as  $\tau$  is increased.<sup>42</sup> This occurs because of the slow signal build-up rates associated with weakly enhanced nuclei residing in the core of particulate solids, and the polarization dynamics can be used to estimate domain size distributions for the particles. Here we use this phenomenon to measure the domain sizes of the particles of amorphous **A** present within the complex superstructure within the formulation **F1**.

Such NMR domain size measurements in complex materials (such as polymer blends) are usually accomplished with  $^1\text{H}$  spin diffusion correlation experiments; however, this requires

resolution of the different phases (or amorphous/crystalline domains) within the directly or indirectly detected  $^1\text{H}$  NMR spectrum.<sup>92</sup> For example, the molecular level association of APIs and excipients can be confirmed with dipolar HETCOR experiments.<sup>27</sup> Carbon-13 detected proton  $T_1$  measurements for excipients and API signals are also useful to place an upper limit on the size of API domains: the observation of distinct  $T_1$ 's for the API and excipients proves phase separation, while the observation of a common  $T_1$  usually suggests that the API exists in domains smaller than 100 nm that are well mixed with the excipient(s).<sup>27</sup> Munson and co-workers have previously demonstrated that *qualitative* measurements of domain (crystallite) sizes in pharmaceutical solids can be obtained by measuring proton  $T_1$ 's and/or measuring the  $^{13}\text{C}$  peak widths to quantify anisotropic bulk magnetic susceptibility (ABMS).<sup>41,93</sup> However, domain sizes have never been directly measured by NMR for a formulated pharmaceutical compound. The advantage of the DNP based method is that no  $^1\text{H}$  chemical shift differences are required; rather, only CP signal build-ups with and without microwaves need to be observed. For these experiments, **F1** was packed into a thin wall 3.2 mm zirconia rotor to maximize sensitivity in the experiments without DNP. Poorer microwave transmission through the zirconia rotor<sup>94</sup> leads to the reduced values of  $\epsilon_{CP}$  for **F1** reported in Figure 4.



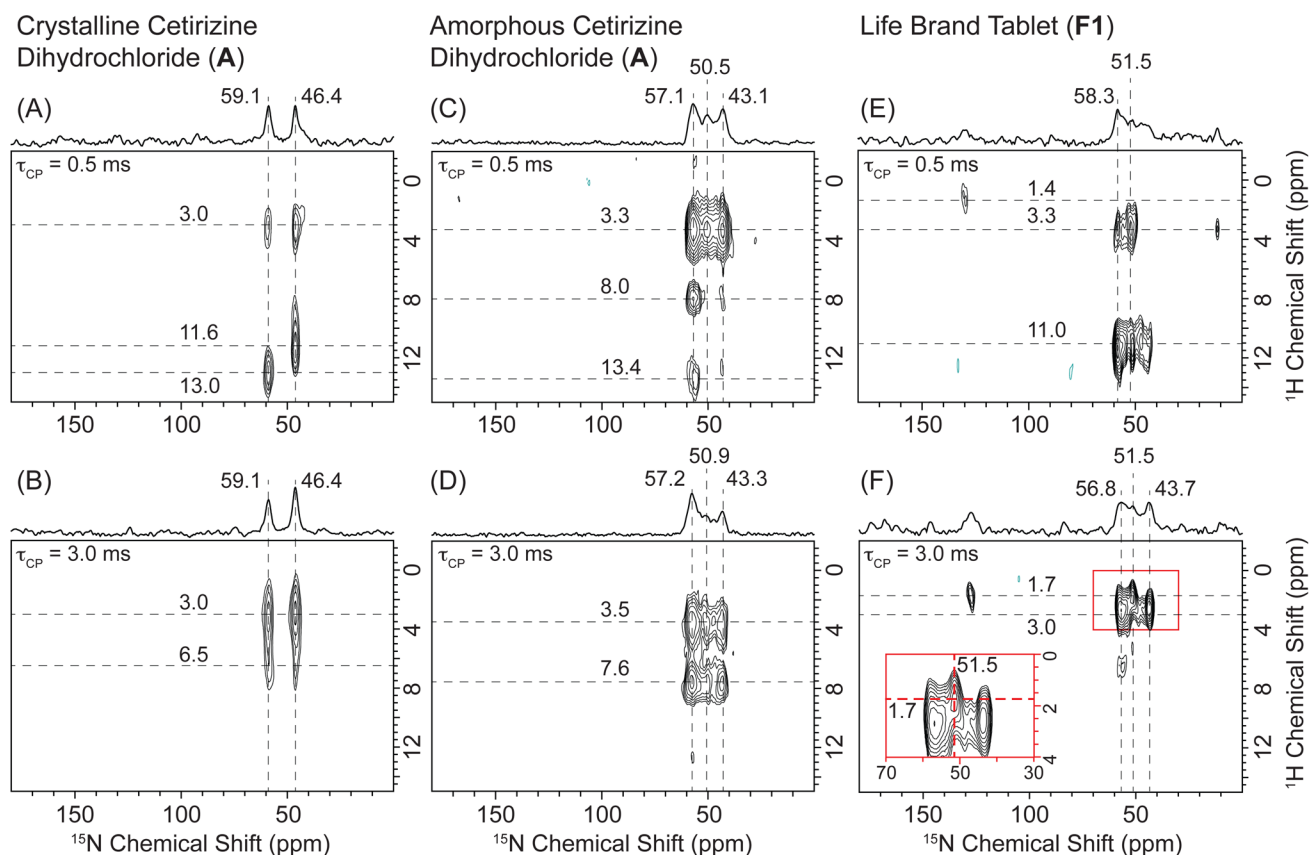


**Figure 5.** Natural abundance DNP enhanced  $^1\text{H}$ – $^{15}\text{N}$  dipolar HETCOR spectra of crystalline **A** (A and B), amorphous **A** (C and D), and **F1** (E and F). The spectra were acquired with contact times ( $\tau_{\text{CP}}$ ) of 0.5 ms (top spectra) and 3.0 ms (lower spectra) to probe for short- and long-range  $^1\text{H}$ – $^{15}\text{N}$  distances, respectively. Key  $^{15}\text{N}$  chemical shifts and  $^1\text{H}$  correlations are indicated on the spectra with dashed lines. An expanded view of the correlations is provided for part F. HETCOR spectra of crystalline **A** were acquired with 4 scans per increment, an 8 s polarization delay, 52 individual  $t_1$  increments, and a  $64\ \mu\text{s}$   $t_1$  increment (27 min each). HETCOR spectra of amorphous **A** were acquired with (C) 64 or (D) 48 scans per increment, a 5.2 s polarization delay, 64 individual  $t_1$  increments, and a  $64\ \mu\text{s}$   $t_1$  increment (5.2 and 4.4 h, respectively). HETCOR spectra of **F1** were acquired with 128 scans (E) or 96 scans (F) per increment, a 3 s polarization delay, 52 individual  $t_1$  increments, and a  $64\ \mu\text{s}$   $t_1$  increment (5.5 and 4.2 h, respectively). During  $t_1$ ,  $\epsilon\text{DUMBO-1}_{22}$  homonuclear  $^1\text{H}$  dipolar decoupling<sup>86</sup> was applied and proton chemical shifts were corrected by applying a scaling factor of 0.57. The States-TPPI procedure<sup>88,89</sup> was employed to achieve quadrature detection in the indirect dimension.

As shown in Figure 4A and B, similar to previous observations for crystalline solids, we observed stretched exponential signal build-ups and a significant variation in  $\epsilon_{\text{CP}}$  for the aromatic API carbon resonances as a function of  $\tau$ . This clearly indicates that **A** exists in distinct particulate domains within **F1** and that the API is externally polarized through proton spin diffusion.<sup>42</sup> Using our previously developed numerical model of the diffusion equation, we can simulate the signal build-up rates and variation in  $\epsilon$  with  $\tau$  for different particle size ranges. We assume that the proton longitudinal relaxation time within the amorphous **A** particles is 5.3 s based upon a measurement of the proton  $T_1$  for amorphous **A** in **F1** in the absence of added radical solution at 110 K (Figure S12, Supporting Information). The enhancement at the surface of the API particles ( $\epsilon_0$ ) was assumed to be equal to the  $\epsilon_{\text{CP}}$  value measured for the **P** resonance at 41.5 ppm, which was found to be 43(7) (Figure 4C). This assumption was made because the enhancement for **A** is similar (but less than) the enhancement for **P** at short polarization delays. The enhancement for **P** does not decrease with the polarization delay (within the uncertainty of the measurements), and DNP experiments on pure impregnated **P** also indicate that the biradical solution is directly incorporated into the polymer. The spin diffusion constant ( $D$ ) was assumed

to be equal to  $1.0 \times 10^5\ \text{\AA}^2\ \text{s}^{-1}$ , a value typical of fully protonated organic solids.<sup>77</sup> Using these parameters, simulations of  $\epsilon$  as a function of  $\tau$  with uniform radius particles provide the best agreement for 0.3  $\mu\text{m}$  radius particles (Figure 4D).

Single particle simulations were also performed with  $D$  values between  $1.0 \times 10^5$  and  $1.0 \times 10^4\ \text{\AA}^2\ \text{s}^{-1}$  (typical values for organic solids)<sup>77,95</sup> to explore the influence of  $D$  on the predicted particle size. As expected, if the particle radius is held constant at 0.3  $\mu\text{m}$ , then the calculated values of  $\epsilon$  decrease as  $D$  decreases (Figure S13A, Supporting Information). On the other hand, for reduced  $D$  values of  $1.0 \times 10^4$  and  $5.0 \times 10^4\ \text{\AA}^2\ \text{s}^{-1}$ , better agreement with experiment is realized for smaller particles with a radius less than 0.3  $\mu\text{m}$  (Figure S13B, Supporting Information). Therefore, if the precise value of  $D$  is unknown, the DNP based particle size measurements will in principle provide an upper limit on the particle size if a large diffusion constant of  $1.0 \times 10^5\ \text{\AA}^2\ \text{s}^{-1}$  is assumed in the model.

For simulations with (traditional) Weibull distributions<sup>96</sup> of particle radii, we find the agreement is best with an equivalent distribution having a maximum around 0.07  $\mu\text{m}$  (Figure 4E). Note that both the single particle model and Weibull distribution models predict that the majority of particles have radii less than 0.3  $\mu\text{m}$ . We attempted to confirm the DNP solid-

state NMR based API domain size measurements with scanning electron microscopy-energy dispersive X-ray spectroscopy (SEM-EDX) mapping of chlorine within **F1**; however, the measurements were too insensitive because of the low Cl content of **F1**. SEM images of ground **F1** indicate the presence of particles smaller than 1  $\mu\text{m}$  in diameter, which is consistent with the DNP-NMR particle size measurements (Figure S14, Supporting Information). As discussed above, in the present case, the impregnation procedure may slightly reduce the domain size of **A** due to the partial solubility of amorphous **A** in TCE. For formulations with crystalline API, this should not be an issue.

**3.2.2. Probing API–Excipient Interactions with DNP Enhanced Solid-State NMR.** For all formulations, both the  $^{13}\text{C}$  and  $^{15}\text{N}$  resonances of the API are much broader than those observed for the corresponding DNP enhanced spectra of crystalline **A** (Figure 3). The observed chemical shifts and breadths of the observed resonances are similar to those observed for pure amorphous **A**, consistent with an amorphous phase of **A** within the formulations. The DNP enhanced  $^{15}\text{N}$  CPMAS spectra of **F1–F4** possess two separated broad features with shifts centered around ca. 58 and 44 ppm. Additional broad  $^{15}\text{N}$  sites with shifts between 54 and 51 ppm are also clearly visible for **F1–F4** and amorphous **A**.

Natural abundance 2D  $^1\text{H}$ – $^{15}\text{N}$  HETCOR spectra of crystalline and amorphous **A** and **F1** are shown in Figure 5. 2D  $^1\text{H}$ – $^{15}\text{N}$  HETCOR NMR spectra were acquired for **F1**, since it had the highest API wt %, although sensitivity is high enough that 2D  $^{15}\text{N}$  NMR spectra could also be acquired for the other formulations. The  $^1\text{H}$ – $^{15}\text{N}$  HETCOR spectrum of **F1** acquired with a 3.0 ms contact time shown in Figure 5F indicates the presence of a  $^{15}\text{N}$  chemical shift for **A** centered at 51.5 ppm. This  $^{15}\text{N}$  chemical shift was not observed in the  $^{15}\text{N}$  CPMAS spectra of crystalline **A**, but a similar chemical shift is observed in spectra of amorphous **A**. Within **F1**, the site at 51.5 ppm correlates to  $^1\text{H}$  nuclei with chemical shifts of 1.7 ppm (and other aliphatic protons with shifts  $>2.0$  ppm). Importantly, this correlation is not observed in the HETCOR spectra of amorphous **A** alone.  $^1\text{H}$ – $^{13}\text{C}$  and  $^1\text{H}$ – $^{15}\text{N}$  HETCOR spectra of **P** show that the  $^1\text{H}$  nuclei of **P** possess shifts between 1.0 and 1.8 ppm (Figure S10, Supporting Information), while all the  $^1\text{H}$  nuclei in both amorphous and crystalline **A** possess chemical shifts greater than 2.7 ppm. Therefore, the  $^1\text{H}$ – $^{15}\text{N}$  correlation at 1.7 and 51.5 ppm indicates that a small amount of **A** is in contact with **P** (likely through dispersive forces and/or hydrogen bonding interactions).<sup>30,37–40</sup> As discussed above, amorphous **A** exists within small sub- $\mu\text{m}$  domains within **F1**. The  $^{15}\text{N}$  resonance at 51.5 ppm likely corresponds to molecules of **A** at the surface of the amorphous API particles which interact with **P**.  $^1\text{H}$ – $^{13}\text{C}$  HETCOR spectra of **F1** do not unambiguously show correlations between the povidone carbon nuclei and the protons of **A** (Figure S3, Supporting Information) because these key correlations are obscured in the crowded  $^1\text{H}$  and  $^{13}\text{C}$  spectra. This demonstrates one of the advantages of  $^{15}\text{N}$  solid-state NMR for the analysis of pharmaceutical formulations. Finally, we note that as discussed above solution  $^1\text{H}$  NMR spectra of extracts of **F4** in an excess of TCE show signals from **A** (Figures S6 and S15, Supporting Information). However, in the solution  $^1\text{H}$  NMR spectrum, the peaks of **A** and **P** are both significantly broadened, suggesting that the **A** observed in solution is associated with **P**, consistent with the hypotheses above regarding **A–P** intermolecular interactions.

## 4. CONCLUSIONS

In summary, impregnation DNP enables the expedient acquisition of 1D and 2D natural abundance  $^{15}\text{N}$  and  $^{13}\text{C}$  solid-state NMR spectra of pure organic solids and formulated APIs. This overcomes the sensitivity limitation for formulations with low API contents. The impregnation method is extremely simple, and the only requirement is the identification of a solvent that does not dissolve the API and is compatible with DNP. In the present case, the amorphous API was found to be slightly soluble within the impregnating solution but not to the extent that it prevented the study. With state of the art polarizing agents,<sup>79</sup> sensitivity enhancements of 2 orders of magnitude were obtained for the commercial formulations examined here. The ability to rapidly acquire both  $^{13}\text{C}$  and  $^{15}\text{N}$  multidimensional CPMAS NMR spectra should aid NMR crystallography studies of bulk solids *in situ* and provide novel structural insight into formulated pharmaceuticals. In this instance, we immediately identified that the API was present in an amorphous form, and by analyzing the variation in DNP enhancement with polarization delay, it was possible to straightforwardly determine the distribution of API particle sizes present within the complex superstructure of the formulated samples. Furthermore, using high-sensitivity  $^1\text{H}$ – $^{15}\text{N}$  correlation NMR spectra, we were able to identify characteristic  $^{15}\text{N}$  resonances corresponding to API molecules interacting with the excipient. Measuring domain sizes *in situ* and API–excipient interactions are some of the most challenging parameters to measure by conventional means.

Since DNP enhancements can vary between different components, these experiments do not provide easy access to quantitative measures of composition. In cases where multiple phases of the API are present (e.g., multiple polymorphs, crystalline vs amorphous, molecular vs aggregated, etc.), we expect that quantification of the API phase by NMR is best performed with conventional 1D  $^{13}\text{C}$  CPMAS NMR spectra. However, with DNP enhanced solid-state NMR, it should be possible to rapidly identify API polymorphs in formulations (including trace amounts of secondary phases), perform *in situ* NMR crystallography, and/or study the aging of formulations, etc. In particular, the method is well suited for the characterization of APIs with long proton longitudinal relaxation times,<sup>42</sup> something that is extremely challenging for conventional NMR experiments.

## ■ ASSOCIATED CONTENT

### ■ Supporting Information

Details on sample preparations, additional 1D and 2D NMR spectra, SEM images, and MatLab code for the numerical calculations. This material is available free of charge via the Internet at <http://pubs.acs.org>.

## ■ AUTHOR INFORMATION

### Corresponding Author

lyndon.emsley@ens-lyon.fr

### Notes

The authors declare no competing financial interest.

## ■ ACKNOWLEDGMENTS

We are grateful to Dr. Fabien Aussenac for his assistance with all of the DNP solid-state NMR experiments. We would like to thank Drs. Werner Maas, Alain Belguise, Melanie Rosay, and Bruker for providing access to the DNP solid-state NMR

spectrometer. Dr. David Gajan is thanked for assistance with some DNP experiments. We thank the EMEZ center and Dr. F. Krumeich for acquiring SEM images. A.J.R. acknowledges support from a EU Marie-Curie IIF Fellowship (PIIF-GA-2010-274574). C.M.W. acknowledges the Natural Sciences and Engineering Research Council (NSERC) of Canada for a postdoctoral fellowship. Financial support is acknowledged from the Agence Nationale de la Recherche grant ANR-2010-BLAN-0806-01, EQUIPEX contract ANR-10-EQPX-47-01, SNF project number 200021\_134775/1, ERC Advanced Grant No. 320860, and the ETH Zürich. We thank Prof. Paul Tordo, Dr. Olivier Ouari and Dr. Gilles Casano (Aix-Marseille Université) for supplying the TEKPol and bCTbK biradicals.

## REFERENCES

- (1) Threlfall, T. L. *Analyst* **1995**, *120*, 2435–2460.
- (2) Bernstein, J. *Polymorphism in Molecular Crystals*; Oxford University Press: Oxford, U.K., 2002.
- (3) Harris, R. K. *Analyst* **2006**, *131*, 351–373.
- (4) Berendt, R. T.; Sperger, D. M.; Isbester, P. K.; Munson, E. J. *TrAC, Trends Anal. Chem.* **2006**, *25*, 977–984.
- (5) Vogt, F. G. *Future Med. Chem.* **2010**, *2*, 915–921.
- (6) Brown, S. P.; Zhu, X. X.; Saalwachter, K.; Spiess, H. W. *J. Am. Chem. Soc.* **2001**, *123*, 4275–4285.
- (7) Elena, B.; Emsley, L. *J. Am. Chem. Soc.* **2005**, *127*, 9140–9146.
- (8) Brouwer, D. H.; Darton, R. J.; Morris, R. E.; Levitt, M. H. *J. Am. Chem. Soc.* **2005**, *127*, 10365–10370.
- (9) Seidel, K.; Etzkorn, M.; Sonnenberg, L.; Griesinger, C.; Sebald, A.; Baldus, M. *J. Phys. Chem. A* **2005**, *109*, 2436–2442.
- (10) Elena, B.; Pintacuda, G.; Mifsud, N.; Emsley, L. *J. Am. Chem. Soc.* **2006**, *128*, 9555–9560.
- (11) Facelli, J. C.; Grant, D. M. *Nature* **1993**, *365*, 325–327.
- (12) Ochsenfeld, C.; Brown, S. P.; Schnell, I.; Gauss, J.; Spiess, H. W. *J. Am. Chem. Soc.* **2001**, *123*, 2597–2606.
- (13) Rapp, A.; Schnell, I.; Sebastiani, D.; Brown, S. P.; Percec, V.; Spiess, H. W. *J. Am. Chem. Soc.* **2003**, *125*, 13284–13297.
- (14) Pickard, C. J.; Salager, E.; Pintacuda, G.; Elena, B.; Emsley, L. *J. Am. Chem. Soc.* **2007**, *129*, 8932–8933.
- (15) Cadars, S.; Brouwer, D. H.; Chmelka, B. F. *Phys. Chem. Chem. Phys.* **2009**, *11*, 1825–1837.
- (16) Salager, E.; Stein, R. S.; Pickard, C. J.; Elena, B.; Emsley, L. *Phys. Chem. Chem. Phys.* **2009**, *11*, 2610–2621.
- (17) Salager, E.; Day, G. M.; Stein, R. S.; Pickard, C. J.; Elena, B.; Emsley, L. *J. Am. Chem. Soc.* **2010**, *132*, 2564–2565.
- (18) Perras, F. A.; Bryce, D. L. *J. Phys. Chem. C* **2012**, *116*, 19472–19482.
- (19) Mafra, L.; Santos, S. M.; Siegel, R.; Alves, I.; Almeida Paz, F. A.; Dudenko, D.; Spiess, H. W. *J. Am. Chem. Soc.* **2012**, *134*, 71–74.
- (20) Baías, M.; Widdifield, C. M.; Dumez, J.-N.; Thompson, H. P. G.; Cooper, T. G.; Salager, E.; Bassil, S.; Stein, R. S.; Lesage, A.; Day, G. M.; Emsley, L. *Phys. Chem. Chem. Phys.* **2013**, *15*, 8069–8080.
- (21) Brouwer, D. H.; Cadars, S.; Eckert, J.; Liu, Z.; Terasaki, O.; Chmelka, B. F. *J. Am. Chem. Soc.* **2013**, *135*, 5641–5655.
- (22) Baías, M.; Dumez, J.-N.; Svensson, P. H.; Schantz, S.; Day, G. M.; Emsley, L. *J. Am. Chem. Soc.* **2013**, *135*, 17501–17507.
- (23) Wenslow, R. M. *Drug Dev. Ind. Pharm.* **2002**, *28*, 555–561.
- (24) Hamaed, H.; Pawlowski, J. M.; Cooper, B. F. T.; Fu, R.; Eichhorn, S. H.; Schurko, R. W. *J. Am. Chem. Soc.* **2008**, *130*, 11056–11065.
- (25) Katrincic, L. M.; Sun, Y. T.; Carlton, R. A.; Diederich, A. M.; Mueller, R. L.; Vogt, F. G. *Int. J. Pharm.* **2009**, *366*, 1–13.
- (26) Hung, I.; Uldry, A. C.; Becker-Baldus, J.; Webber, A. L.; Wong, A.; Smith, M. E.; Joyce, S. A.; Yates, J. R.; Pickard, C. J.; Dupree, R.; Brown, S. P. *J. Am. Chem. Soc.* **2009**, *131*, 1820–1834.
- (27) Pham, T. N.; Watson, S. A.; Edwards, A. J.; Chavda, M.; Clawson, J. S.; Strohmeier, M.; Vogt, F. G. *Mol. Pharmaceutics* **2010**, *7*, 1667–1691.
- (28) O'Dell, L. A.; Schurko, R. W.; Harris, K. J.; Autschbach, J.; Ratcliffe, C. I. *J. Am. Chem. Soc.* **2011**, *133*, 527–546.
- (29) Bonhomme, C.; Gervais, C.; Folliet, N.; Pourpoint, F.; Diogo, C. C.; Lao, J.; Jallot, E.; Lacroix, J.; Nedelec, J. M.; Iuga, D.; Hanna, J. V.; Smith, M. E.; Xiang, Y.; Du, J. C.; Laurencin, D. *J. Am. Chem. Soc.* **2012**, *134*, 12611–12628.
- (30) Tatton, A. S.; Pham, T. N.; Vogt, F. G.; Iuga, D.; Edwards, A. J.; Brown, S. P. *CrystEngComm* **2012**, *14*, 2654–2659.
- (31) Burgess, K. M. N.; Perras, F. A.; Lebrun, A.; Messner-Henning, E.; Korobkov, I.; Bryce, D. L. *J. Pharm. Sci.* **2012**, *101*, 2930–2940.
- (32) Kong, X. Q.; O'Dell, L. A.; Terskikh, V.; Ye, E.; Wang, R. Y.; Wu, G. *J. Am. Chem. Soc.* **2012**, *134*, 14609–14617.
- (33) Haimovich, A.; Eliav, U.; Goldbourt, A. *J. Am. Chem. Soc.* **2012**, *134*, 5647–5651.
- (34) Vogt, F. G.; Yin, H.; Forcino, R. G.; Wu, L. *Mol. Pharmacol.* **2013**, *10*, 3433–3446.
- (35) Kong, X. Q.; Shan, M.; Terskikh, V.; Hung, I.; Gan, Z. H.; Wu, G. *J. Phys. Chem. B* **2013**, *117*, 9643–9654.
- (36) Umino, M.; Higashi, K.; Masu, H.; Limwikrant, W.; Yamamoto, K.; Moribe, K. *J. Pharm. Sci.* **2013**, *102*, 2738–2747.
- (37) Saindon, P. J.; Cauchon, N. S.; Sutton, P. A.; Chang, C. J.; Peck, G. E.; Byrn, S. R. *Pharm. Res.* **1993**, *10*, 197–203.
- (38) Lubach, J. W.; Padden, B. E.; Winslow, S. L.; Salisbury, J. S.; Masters, D. B.; Topp, E. M.; Munson, E. J. *Anal. Bioanal. Chem.* **2004**, *378*, 1504–1510.
- (39) Harris, R. K.; Hodgkinson, P.; Larsson, T.; Muruganatham, A. *J. Pharm. Biomed. Anal.* **2005**, *38*, 858–864.
- (40) Tobyn, M.; Brown, J.; Dennis, A. B.; Fakes, M.; Gao, Q.; Gamble, J.; Khimyak, Y. Z.; McGeorge, G.; Patel, C.; Sinclair, W.; Timmins, P.; Yin, S. *J. Pharm. Sci.* **2009**, *98*, 3456–3468.
- (41) Lubach, J. W.; Xu, D.; Segmuller, B. E.; Munson, E. J. *J. Pharm. Sci.* **2007**, *96*, 777–787.
- (42) Rossini, A. J.; Zagdoun, A.; Hegner, F. S.; Schwarzwälder, M.; Gajan, D.; Copéret, C.; Lesage, A.; Emsley, L. *J. Am. Chem. Soc.* **2012**, *134*, 16899–16908.
- (43) Chang, C. J.; Diaz, L. E.; Morin, F.; Grant, D. M. *Magn. Reson. Chem.* **1986**, *24*, 768–771.
- (44) Diaz, L. E.; Frydman, L.; Olivieri, A. C.; Frydman, B. *Anal. Lett.* **1987**, *20*, 1657–1666.
- (45) Jagannathan, N. R. *Curr. Sci.* **1987**, *56*, 827–830.
- (46) Sanchez, S.; Ziarelli, F.; Viel, S.; Delaurent, C.; Caldarelli, S. *J. Pharm. Biomed. Anal.* **2008**, *47*, 683–687.
- (47) Griffin, J. M.; Martin, D. R.; Brown, S. P. *Angew. Chem., Int. Ed.* **2007**, *46*, 8036–8038.
- (48) Zhou, D. H.; Rienstra, C. M. *Angew. Chem., Int. Ed.* **2008**, *47*, 7328–7331.
- (49) Tatton, A. S.; Pham, T. N.; Vogt, F. G.; Iuga, D.; Edwards, A. J.; Brown, S. P. *Mol. Pharmacol.* **2013**, *10*, 999–1007.
- (50) Zhou, D. H.; Shah, G.; Mullen, C.; Sandoz, D.; Rienstra, C. M. *Angew. Chem., Int. Ed.* **2009**, *48*, 1253–1256.
- (51) Nishiyama, Y.; Frey, M. H.; Mukasa, S.; Utsumi, H. *J. Magn. Reson.* **2010**, *202*, 135–139.
- (52) Zielinska-Pisklak, M.; Pisklak, D. M.; Wawer, I. *J. Pharm. Sci.* **2012**, *101*, 1763–1772.
- (53) Vogt, F. G.; Williams, G. R. *Pharm. Res.* **2012**, *29*, 1866–1881.
- (54) Kelley, W. P.; Chen, S. J.; Floyd, P. D.; Hu, P.; Kapsi, S. G.; Kord, A. S.; Sun, M. J.; Vogt, F. G. *Anal. Chem.* **2012**, *84*, 4357–4372.
- (55) Vogt, F. G.; Strohmeier, M. *Mol. Pharm.* **2012**, *9*, 3357–3374.
- (56) Maly, T.; Debelouchina, G. T.; Bajaj, V. S.; Hu, K. N.; Joo, C. G.; Mak-Jurkauskas, M. L.; Sirigiri, J. R.; van der Wel, P. C. A.; Herzfeld, J.; Temkin, R. J.; Griffin, R. G. *J. Chem. Phys.* **2008**, *128*, 052211.
- (57) Ni, Q. Z.; Daviso, E.; Can, T. V.; Markhasin, E.; Jawla, S. K.; Swager, T. M.; Temkin, R. J.; Herzfeld, J.; Griffin, R. G. *Acc. Chem. Res.* **2013**, *48*, 1933–1941.



- (58) Mak-Jurkauskas, M. L.; Bajaj, V. S.; Hornstein, M. K.; Belenky, M.; Griffin, R. G.; Herzfeld, J. *Proc. Natl. Acad. Sci. U.S.A.* **2008**, *105*, 883–888.
- (59) Salnikov, E.; Rosay, M.; Pawsey, S.; Ouari, O.; Tordo, P.; Bechinger, B. J. *Am. Chem. Soc.* **2010**, *132*, 5940–5941.
- (60) Sergeyev, I. V.; Day, L. A.; Goldbourt, A.; McDermott, A. E. *J. Am. Chem. Soc.* **2011**, *133*, 20208–20217.
- (61) Linden, A. H.; Lange, S.; Franks, W. T.; Akbey, U.; Specker, E.; van Rossum, B.-J.; Oschkinat, H. *J. Am. Chem. Soc.* **2011**, *133*, 19266–19269.
- (62) Reggie, L.; Lopez, J. J.; Collinson, I.; Glaubitz, C.; Lorch, M. J. *Am. Chem. Soc.* **2011**, *133*, 19084–19086.
- (63) Potapov, A.; Yau, W.-M.; Tycko, R. *J. Magn. Reson.* **2013**, *231*, 5–14.
- (64) Takahashi, H.; Ayala, I.; Bardet, M.; De Paepe, G.; Simorre, J. P.; Hediger, S. J. *Am. Chem. Soc.* **2013**, *135*, 5105–5110.
- (65) Wang, T.; Park, Y. B.; Caporini, M. A.; Rosay, M.; Zhong, L. H.; Cosgrove, D. J.; Hong, M. *Proc. Natl. Acad. Sci. U.S.A.* **2013**, *110*, 16444–16449.
- (66) Lesage, A.; Lelli, M.; Gajan, D.; Caporini, M. A.; Vitzthum, V.; Mieville, P.; Alauzun, J.; Roussey, A.; Thieuleux, C.; Mehdi, A.; Bodenhausen, G.; Copéret, C.; Emsley, L. *J. Am. Chem. Soc.* **2010**, *132*, 15459–15461.
- (67) Lelli, M.; Gajan, D.; Lesage, A.; Caporini, M. A.; Vitzthum, V.; Mieville, P.; Heroguel, F.; Rascon, F.; Roussey, A.; Thieuleux, C.; Boualleg, M.; Veyre, L.; Bodenhausen, G.; Copéret, C.; Emsley, L. *J. Am. Chem. Soc.* **2011**, *133*, 2104–2107.
- (68) Lafon, O.; Rosay, M.; Aussenac, F.; Lu, X.; Trebosc, J.; Cristini, O.; Kinowski, C.; Touati, N.; Vezin, H.; Amoureux, J. P. *Angew. Chem., Int. Ed.* **2011**, *50*, 8367–8370.
- (69) Rossini, A. J.; Zagdoun, A.; Lelli, M.; Canivet, J.; Aguado, S.; Ouari, O.; Tordo, P.; Rosay, M.; Maas, W. E.; Copéret, C.; Farrusseng, D.; Emsley, L.; Lesage, A. *Angew. Chem., Int. Ed.* **2012**, *51*, 123–127.
- (70) Zagdoun, A.; Casano, G.; Ouari, O.; Lapadula, G.; Rossini, A. J.; Lelli, M.; Baffert, M.; Gajan, D.; Veyre, L.; Maas, W. E.; Rosay, M.; Weber, R. T.; Thieuleux, C.; Copéret, C.; Lesage, A.; Tordo, P.; Emsley, L. *J. Am. Chem. Soc.* **2012**, *134*, 2284–2291.
- (71) Takahashi, H.; Lee, D.; Dubois, L.; Bardet, M.; Hediger, S.; De Paëpe, G. *Angew. Chem., Int. Ed.* **2012**, *124*, 11936–11939.
- (72) Rossini, A. J.; Zagdoun, A.; Lelli, M.; Lesage, A.; Copéret, C.; Emsley, L. *Acc. Chem. Res.* **2013**, *46*, 1942–1951.
- (73) Blanc, F.; Sperrin, L.; Jefferson, D. A.; Pawsey, S.; Rosay, M.; Grey, C. P. *J. Am. Chem. Soc.* **2013**, *135*, 2975–2978.
- (74) Lafon, O.; Thankamony, A. S. L.; Kobayashi, T.; Carnevale, D.; Vitzthum, V.; Slowing, I. I.; Kandel, K.; Vezin, H.; Amoureux, J. P.; Bodenhausen, G.; Pruski, M. *J. Phys. Chem. C* **2013**, *117*, 1375–1382.
- (75) Blanc, F.; Chong, S. Y.; McDonald, T. O.; Adams, D. J.; Pawsey, S.; Caporini, M. A.; Cooper, A. I. *J. Am. Chem. Soc.* **2013**, *135*, 15290–15293.
- (76) Song, C. S.; Hu, K. N.; Joo, C. G.; Swager, T. M.; Griffin, R. G. *J. Am. Chem. Soc.* **2006**, *128*, 11385–11390.
- (77) van der Wel, P. C. A.; Hu, K. N.; Lewandowski, J.; Griffin, R. G. *J. Am. Chem. Soc.* **2006**, *128*, 10840–10846.
- (78) Ong, T. C.; Mak-Jurkauskas, M. L.; Walish, J. J.; Michaelis, V. K.; Corzilius, B.; Smith, A. A.; Clausen, A. M.; Cheetham, J. C.; Swager, T. M.; Griffin, R. G. *J. Phys. Chem. B* **2013**, *117*, 3040–3046.
- (79) Zagdoun, A.; Casano, G.; Ouari, O.; Schwarzwälder, M.; Rossini, A. J.; Aussenac, F.; M., Y.; G., J.; Copéret, C.; Lesage, A.; Tordo, P.; Emsley, L. *J. Am. Chem. Soc.* **2013**, *135*, 12790–12797.
- (80) Zagdoun, A.; Casano, G.; Ouari, O.; Lapadula, G.; Rossini, A. J.; Lelli, M.; Baffert, M.; Gajan, D.; Veyre, L.; Maas, W. E.; Rosay, M.; Weber, R. T.; Thieuleux, C.; Copéret, C.; Lesage, A.; Tordo, P.; Emsley, L. *J. Am. Chem. Soc.* **2012**, *134*, 2284–2291.
- (81) Rosay, M.; Tometich, L.; Pawsey, S.; Bader, R.; Schauwecker, R.; Blank, M.; Borchard, P. M.; Cauffman, S. R.; Felch, K. L.; Weber, R. T.; Temkin, R. J.; Griffin, R. G.; Maas, W. E. *Phys. Chem. Chem. Phys.* **2010**, *12*, 5850–5860.
- (82) Harris, R. K.; Becker, E. D.; De Menezes, S. M. C.; Goodfellow, R.; Granger, P. *Pure Appl. Chem.* **2001**, *73*, 1795–1818.
- (83) Metz, G.; Wu, X.; Smith, S. J. *Magn. Reson., Ser. A* **1994**, *110*, 219–227.
- (84) Peersen, O.; Wu, X.; Kustanovich, I.; Smith, S. J. *Magn. Reson., Ser. A* **1993**, *104*, 334–339.
- (85) Fung, B. M.; Khitrin, A. K.; Ermolaev, K. J. *Magn. Reson.* **2000**, *142*, 97–101.
- (86) Elena, B.; de Paepe, G.; Emsley, L. *Chem. Phys. Lett.* **2004**, *398*, 532–538.
- (87) Zagdoun, A.; Rossini, A. J.; Gajan, D.; Bourdolle, A.; Ouari, O.; Rosay, M.; Maas, W. E.; Tordo, P.; Lelli, M.; Emsley, L.; Lesage, A.; Copéret, C. *Chem. Commun.* **2011**, *48*, 654–656.
- (88) States, D. J.; Haberkorn, R. A.; Ruben, D. J. *J. Magn. Reson.* **1982**, *48*, 286–292.
- (89) Marion, D.; Wuthrich, K. *Biochem. Biophys. Res. Commun.* **1983**, *113*, 967–974.
- (90) Lesage, A.; Bardet, M.; Emsley, L. *J. Am. Chem. Soc.* **1999**, *121*, 10987–10993.
- (91) Allen, L. V.; Popovich, N. G.; Ansel, H. C. *Ansel's Pharmaceutical Dosage Forms and Drug Delivery Systems*; Wolters Kluwer: Philadelphia, PA, 2011.
- (92) Schmidt-Rohr, K.; Spiess, H. W. *Multidimensional Solid-State NMR and Polymers*, 2nd ed.; Academic Press: London, 1996.
- (93) Barich, D. H.; Davis, J. M.; Schieber, L. J.; Zell, M. T.; Munson, E. J. *J. Pharm. Sci.* **2006**, *95*, 1586–1594.
- (94) Akbey, U.; Franks, W. T.; Linden, A.; Lange, S.; Griffin, R. G.; van Rossum, B. J.; Oschkinat, H. *Angew. Chem., Int. Ed.* **2010**, *49*, 7803–7806.
- (95) Chen, Q.; Schmidt-Rohr, K. *Solid State Nucl. Magn. Reson.* **2006**, *29*, 142–152.
- (96) Weibull, W. J. *Appl. Mech.* **1951**, *18*, 293–297.